Case Studies in Construction Materials 1 (2014) 83–95

Contents lists available at ScienceDirect

Case Studies in Construction Materials

journal homepage: www.elsevier.com/locate/cscm

Case Study

# Case study of first all-GFRP pedestrian bridge in Taiwan

Yeou-Fong Li [a,*], Sainey Badjie [a], Walter W. Chen [a], Yu-Tsung Chiu [b]

[a] Department of Civil Engineering, National Taipei University of Technology, Taiwan
[b] Industrial Technology Research Institute, Material and Chemical Research Laboratory, Taiwan

ARTICLE INFO

*Article history:*
Received 27 January 2014
Received in revised form 28 April 2014
Accepted 5 May 2014
Available online 29 May 2014

*Keywords:*
All-GFRP composite
Pedestrian bridge
ANSYS
Finite element analysis
Case study

ABSTRACT

To forestall the severe deterioration of structures as a result of corrosion, the first all-FRP composite pedestrian bridge was built in Tainan, Taiwan. The bridge superstructure was designed by placing Glass Fiber Reinforced Polymer (GFRP) decks onto four FRP I-girders that served as the bridge girders. Bridge diaphragms and FRP rods placed between the girders helped dissipate the loading to the other girders and prevent torsion respectively. The pultruded GFRP composite profiles were used in constructing this bridge located in the Taijiang National Park of Taiwan. This paper discusses the features of the pedestrian bridge and the detailed design of all the components of the bridge. A new method of digitally archiving the pedestrian bridge using a 3D terrestrial laser scanner was also presented. Lastly, results of the theoretical analysis were compared with the finite element analysis (FEA), to predict the static flexural behavior of an 8-m girder under loadings. After agreement of the theoretical results (using Timoshenko Beam Theory and Euler–Bernoulli Beam Theory) and the FEA results, the pedestrian bridge superstructure was modeled and analyzed. Deflection results obtained from the FEA showed that the pedestrian bridge meets the deflection criteria.



## 1. Introduction

Because Taijiang National Park of Taiwan is located in a chloride concentrated environment, structures made of conventional materials close to the seashore find themselves defenseless to corrosion. After a few years of the construction, steel structural members in the Taijiang National Park are seen to be partly or severely corroded. Handrails in Fig. 1(a) are about a year or two old and have rusted beyond repair while an access ramp to the seaside, in Fig. 1(b), is also affected by the same phenomenon. This raises an alarm and has led to the construction of the pedestrian bridge of high strength, lightweight and environmental resistant Glass Fiber Reinforced Polymer (GFRP) composite as a countermeasure to prevent salt damage.

In fact, GFRP composite materials have been in use on bridges for over a decade now. It is believed that the first GFRP composite pedestrian bridge was built by the Israelis (Tang and Podolny, 1998) in 1975 after which Europe, the U.S. and Asia came into the industry. Europe alone has a great number of pedestrian bridges made of GFRP composite including the famous cable-stayed Aberfeldy Bridge (Skinner, 2009) in Scotland, Fiberline Bridge in Kolding, Denmark (Fiberline Composites, 2013), and Pontresina Bridge in Switzerland (Kutz, 2002). Famous composite bridges for pedestrian use in Asia include the Okinawa Road Park Bridge, Japan (Kitayama and Uno, 2003).

The 8 m-long all-GFRP pedestrian bridge (also known as footbridge) is the first to be built in Taiwan. The main motive for such a bridge was to showcase the superiority of lightweight, high-strength and environmental-resistant GFRP composites

* Corresponding author at: National Taipei University of Technology, 1, Sec. 3, Chung-Xiao E. Road, Taipei 10608, Taiwan. Tel.: +886 2 2771 2171x2648.
*E-mail addresses:* yfli@ntut.edu.tw (Y.-F. Li), saiboy3@hotmail.com (S. Badjie), waltchen@ntut.edu.tw (W.W. Chen), yutschiu@itri.org.tw (Y.-T. Chiu).

http://dx.doi.org/10.1016/j.cscm.2014.05.001

(a) Corroded handrails (b) Corroded access ramp

**Fig. 1.** Corrosion problems in Taijiang National Park.

in Civil Engineering. The all-GFRP pedestrian bridge was made of four continuous GFRP I-girders and GFRP decks in its superstructure. Added GFRP diaphragms in the girder-deck system configuration help resist torsion. All other components of the bridge including the handrails, pins and components of the connections were also made of GFRP composites. The design of the bridge adopted the AASHTO's *Guide Specifications for Design of FRP Pedestrian Bridges* (AASHTO, 2008) for the deflection criteria. General inventory data of the pedestrian bridge are as follows:

A. Total length: 8 m;
B. Span length: 7.5 m;
C. Width: 1.5 m;
D. Total weight (Superstructure only): approximately 1.2 tons;
E. Materials: Pultruded GFRP composites and epoxy adhesive;
F. Maximum deflection: $\leq L/500$;
G. Load capacity: 4.07 kN/m$^2$.

In this paper, the detailed installation processes of the all-GFRP pedestrian bridge, including the architectural characteristics, the structural design and installation process is presented. The structural design that includes the deflection requirements and loading conditions follows next. Thereafter, a step-by-step process of assembly and installation of the bridge is briefly recounted. After the introduction, the bridge superstructure is then analyzed by comparing results obtained from theoretical methods (using the Timoshenko Beam theory and the Euler–Bernoulli Beam Theory) with those of finite element analysis (FEA).

This paper also aims to present a new methodology of digitally archiving the structure of the pedestrian bridge. This new methodology utilizes a device called Terrestrial Laser Scanner (TLS), which is a high precision 3D surveying tool that has the ability of recording 3D dimensions of the objects it scanned. The TLS has been adopted for bridge related studies by various researchers. For example, Liu et al. (2012) and Watson et al. (2012) used TLS for measuring bridge clearance, Kayen et al. (2006) and Liu et al. (2011) adopted TLS for detecting damages on bridges, and Chen et al. (2011) used TLS for determining bridge pier displacements during push-over tests. Other works include assessing landslide problems in the Three Gorges Reservoir area of China (Ye et al., 2010), reconstructing landslides in the outskirts of Taipei (Chen et al., 2010), performing topographic analysis of landslides (Hsu and Chen, 2013a,b), and documenting a green campus (Tseng et al., 2013). The TLS has also been used in other areas such as archeology and forestry.

## 2. Aesthetic design

This section discusses, in detail, the architectural design and specifications of the components of the pedestrian bridge.

### 2.1. Bridge type

The bridge is a one span pedestrian bridge, with no camber, spanning 7.5 m from one abutment to the other, a total length of 8 and 1.5 m wide. One end of the bridge is an access ramp entrance in its approach span while the other end (which leads to the sea) has a pedestrian staircase in addition to a wheelchair ramp as shown in Fig. 2(b).

### 2.2. Material design

The pedestrian bridge members were all made of GFRP composite profiles produced by pultrusion by Pulroc Pultrusion (2013) company in Taiwan. The orthotropic material properties provided by the manufacturer (to be used later in the FEA analysis) are shown in Table 1.

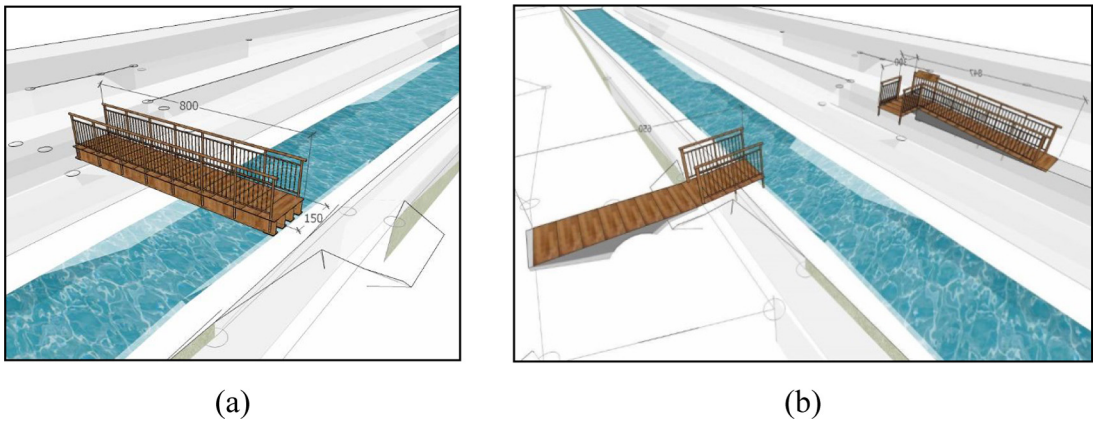


**Fig. 2.** Schematic diagrams of the pedestrian bridge.

**Table 1**
Mechanical properties of the pultruded GFRP components.

| Property[a] | $E_x$ (MPa) | $E_y$ (MPa) | $E_z$ (MPa) | $G_{xy}$ (MPa) | $G_{yz}$ (MPa) | $G_{xz}$ (MPa) | $\nu_{xy}$ | $\nu_{yz}$ | $\nu_{xz}$ |
|---|---|---|---|---|---|---|---|---|---|
| All girders | 6621 | 6621 | 20,690 | 3724 | 3724 | 3724 | 0.33 | 0.11 | 0.11 |
| Diaphragms | 6621 | 20,690 | 6621 | 3724 | 3724 | 3724 | 0.11 | 0.11 | 0.33 |
| Deck plates | 20,690 | 6621 | 6621 | 3724 | 3724 | 3724 | 0.11 | 0.33 | 0.11 |

[a] $X$ = transverse (perpendicular to traffic), $Y$ = vertical direction and $Z$ = longitudinal (traffic) direction.

### 2.3. Girder

The most significant portion of the bridge's superstructure, in this case, is found to be the girders. As stated earlier, four continuous GFRP I-girders, each 800 cm long, 20 cm wide and 41 cm in depth, make up the girders of the pedestrian bridge. The four girders were separated from each other with the use of GFRP diaphragms. These diaphragms were cut sections of the GFRP I-girders. Consequently, the diaphragms will enhance distribution of a concentrated load to other girders (see Fig. 3). Additionally, the GFRP rods would help the pedestrian bridge superstructure to resist torsional loads.

### 2.4. Decking

The GFRP plates measuring 150 cm long, 50 cm wide and 1.2 cm thick were used as bridge deck. They were bonded both mechanically and chemically to the girders of the diaphragm by GFRP pins (diameter = 6 mm) and adhesive resin, respectively.

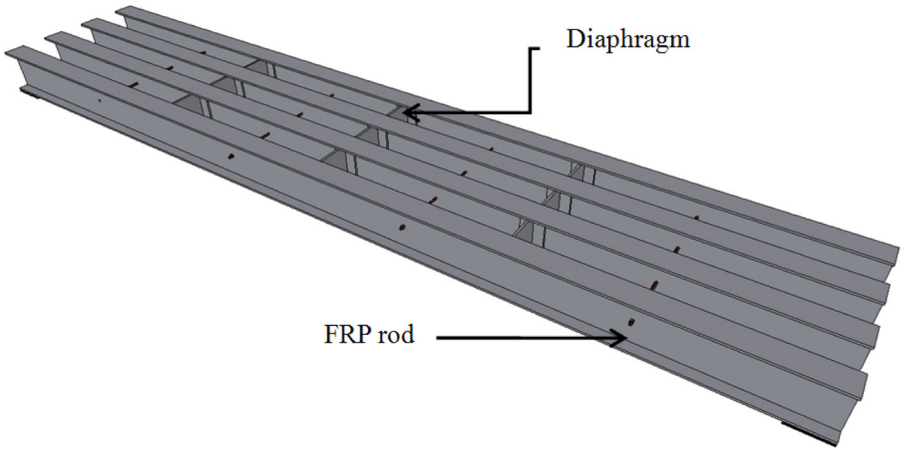


**Fig. 3.** Diaphragm of the pedestrian bridge superstructure.

### 2.5. Handrails

Handrails were provided to a height of 1.1 m above the floor deck to assist pedestrian and those on wheelchairs (see Fig. 4). Pultruded GFRP bars and rods were used. Round GFRP rods, resting on rectangular GFRP battens (40 mm × 15 mm × 3 mm), were placed vertically as spindles in between every two adjacent rectangular newel posts. The spindles serve not only as secondary supports but also to provide stability to the handrail system. It is the newel posts that provide the primary support so it used a bigger cross section (56 mm × 30 mm × 3 mm). In order to provide comfort when users grasp it, a continuous round GFRP bar was chosen for the top cap of both sides of the handrail.

### 2.6. Finishing

For the interior and exterior parts of the bridge, a special environmental resistant paint was used. This paint is also resistant to UV rays. The color chosen was dark brown to harmonize with the natural environment of the park as an existing access ramp nearby was also of the same color.

An anti-skid layer was made by spreading coarse sand over the adhesive resin painted on the floor of the GFRP deck.

### 2.7. Information board

The pedestrian bridge was painted brown to make the whole bridge look as if it was made of steel material, although it is made of GFRP composites. Therefore, to let local users and visitors know of this new technology/material, an information board was provided and placed at the northern end of the bridge.

### 2.8. Abutment

The two bases of abutments were built out of reinforced concrete. GFRP re-bars were used as the reinforcement for the abutment. Rubber bearings were also placed on the abutment under the pedestrian bridge's superstructure.

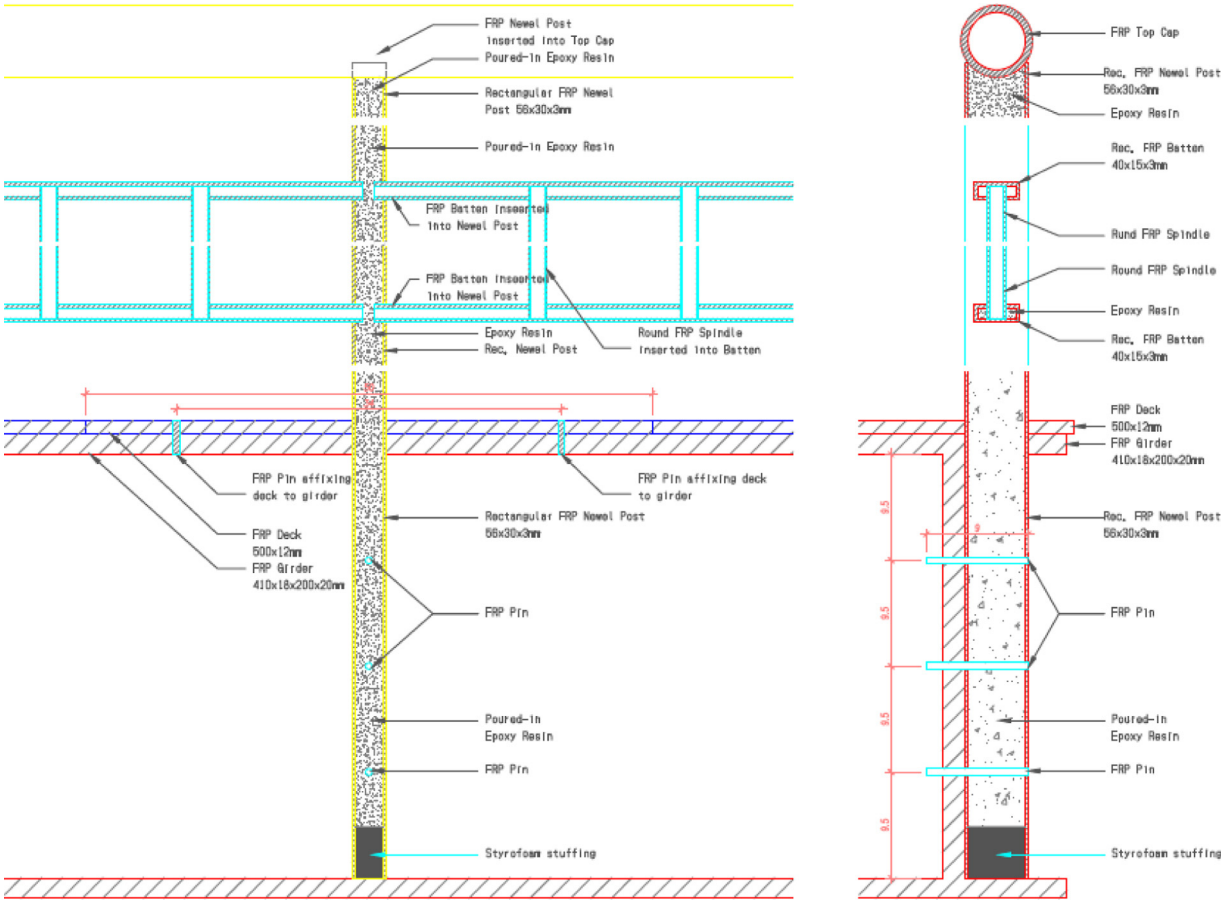


**Fig. 4.** Detailed section view of the pedestrian bridge showing connection between girders and handrail components.

**Table 2**
Deflection criteria of different FRP Bridge design specifications.

| Nation | Spec. name | Issued by | Scope of application | Live load ($kN/m^2$) | Deflection limit |
|---|---|---|---|---|---|
| U.K. | DMFRB Vol. 1, Sec. 3, Part17 (DTD, 2005) | Department of Transport | FRP highway bridges and structures | – | $L/300$ |
| U.S.A. | A Guide to Fiber-Reinforced Polymer Trail Bridges (DAFS, 2006) | Forest Service, U.S. Department of Agriculture | FRP trail bridges | 4.07 | $L/400$ |
| | LRFD Guide Specifications for Design of Pedestrian Bridges (AASHTO, 2009) | AASHTO | Pedestrian bridges | 4.07 | $L/500$ |
| | Guide Specifications for Design of FRP Pedestrian Bridges (AASHTO, 2008) | AASHTO | FRP pedestrian bridges | 4.07 | $L/500$ |
| Japan | Guidelines for Design and Construction of FRP footbridges (JSCE, 2011) | Japan Society of Civil Engineers | FRP footbridges | 5.0 | Main girder $L/500$; other components $L/400$ |

## 3. Structural design

### 3.1. Pedestrian live load

The four GFRP I-girders of the pedestrian bridge were designed for a pedestrian live load of 4.07 $kN/m^2$ of bridge walkway area.

### 3.2. Deflection requirement

Some of the design specifications were followed to design the GFRP composite pedestrian bridges. As seen in Table 2, design specifications mainly from the U.S. and United Kingdom were consulted before the deflection criteria were selected for the pedestrian bridge in the Taijiang National Park. The girders (see Fig. 5) of the pedestrian bridge were designed to meet the deflection goals of AASHTO's *Guide Specifications for Design of FRP Pedestrian Bridges* for a deflection not exceeding $L/500$ (1.5 cm) of the bridge span length.

### 3.3. Connections

All components of the bridge used non-steel materials to avoid any possibility of chloride action on the pedestrian bridge. Both structural members and nonstructural members were connected to one another using environmentally resistant GFRP pins (diameter = 6 mm) in conjunction with high strength epoxy resin adhesive (Figs. 4 and 6).

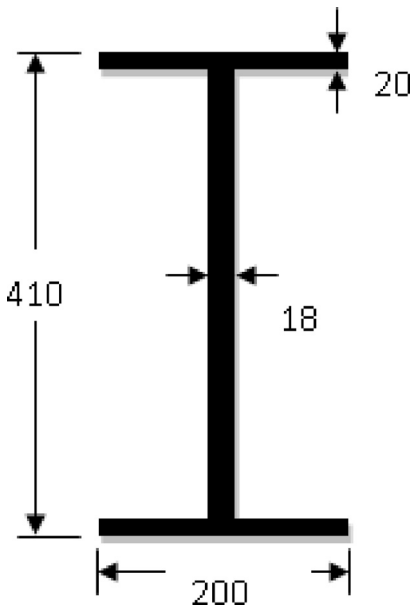


**Fig. 5.** Section of the GFRP girder (units in mm).

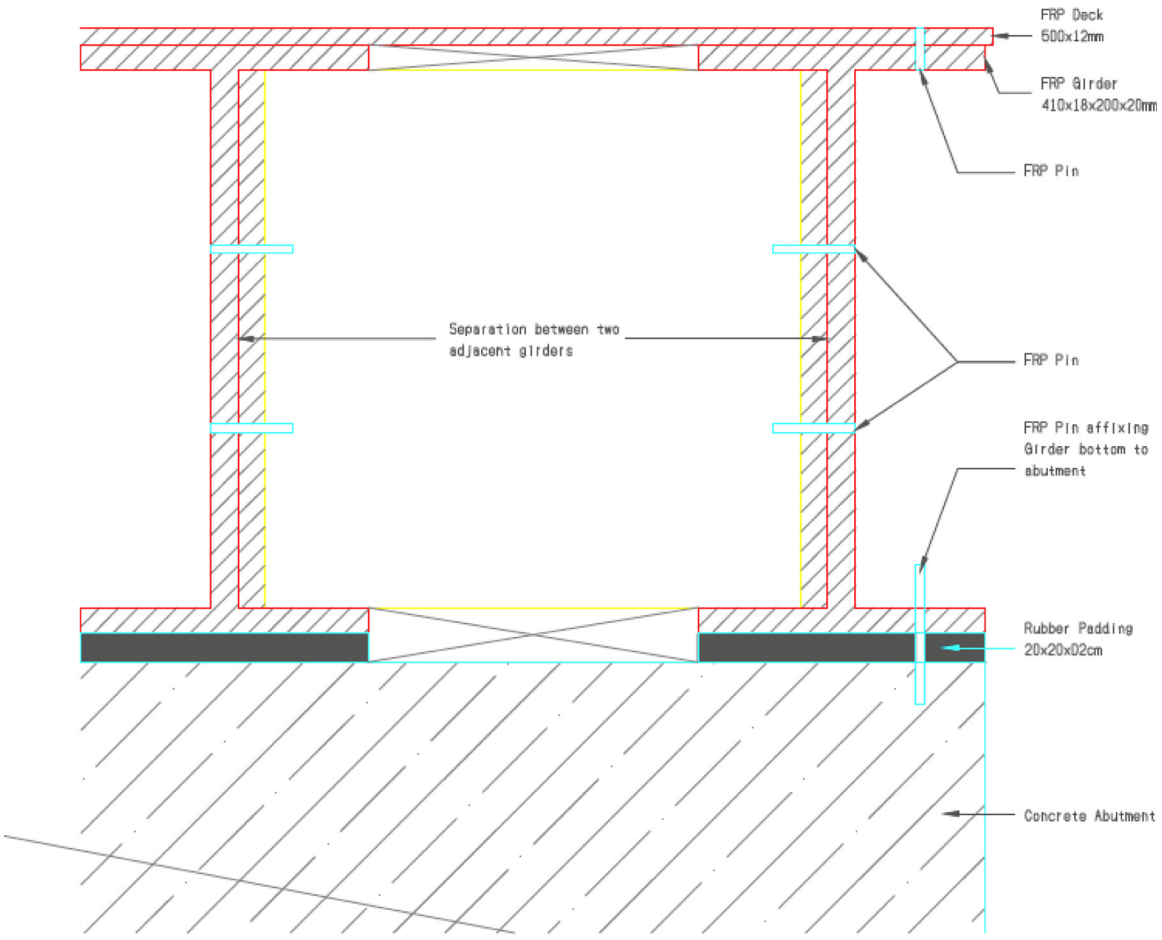


**Fig. 6.** Detailed section view of the pedestrian bridge showing connection between girder, deck and abutment.

## 4. On-site installation

Site investigation and surveying was first carried out. From that, the shape, color and design of the pedestrian bridge were decided. A computer-aided drawing of the pedestrian bridge (Fig. 2) was made to give a more realistic view. Construction began after the different sections of the pultruded GFRP members were delivered to the site from a factory approximately 160 km away. After the members arrived on site, their numbers were confirmed and a visual check was done to assure the members were not damaged during transportation.

Below presents the step-by-step assembly and installation of the pedestrian bridge on-site. A timeline corresponding to the steps is also given in Fig. 7.

1. The GFRP members were cut out in desired sizes and shapes (Fig. 7(a)).
2. A primer was coated on each of the members or to the parts that were to be connected (Fig. 7(b) and (c)). The primer coating acts only as a preparatory coating that enhances adhesion of the epoxy resin to the GFRP members.
3. Holes were drilled on the flanges of the diaphragms and on their connection spots on the web of the GFRP girders (Fig. 7(d)).
4. The surfaces and drilled holes were coated with high-strength epoxy resin adhesive (Fig. 7(e)) before the diaphragms were connected to the four girders using GFRP pins (that serve as screws).
5. The superstructure was then assembled by fixing the GFRP decks on to the assembly (Fig. 7(f)). The surfaces of the decks were initially smoothened, then the primer was applied followed by the epoxy resin adhesive (Fig. 7(g)).
6. Next, components of the handrail including the spindles, newel posts and battens were cut to the desired shapes and sizes (Fig. 7(h)).
7. Assembly of the handrails was then completed by joining its finished components together and to the exterior girders (Fig. 7(i)) with the help of the high-strength epoxy resin adhesive.

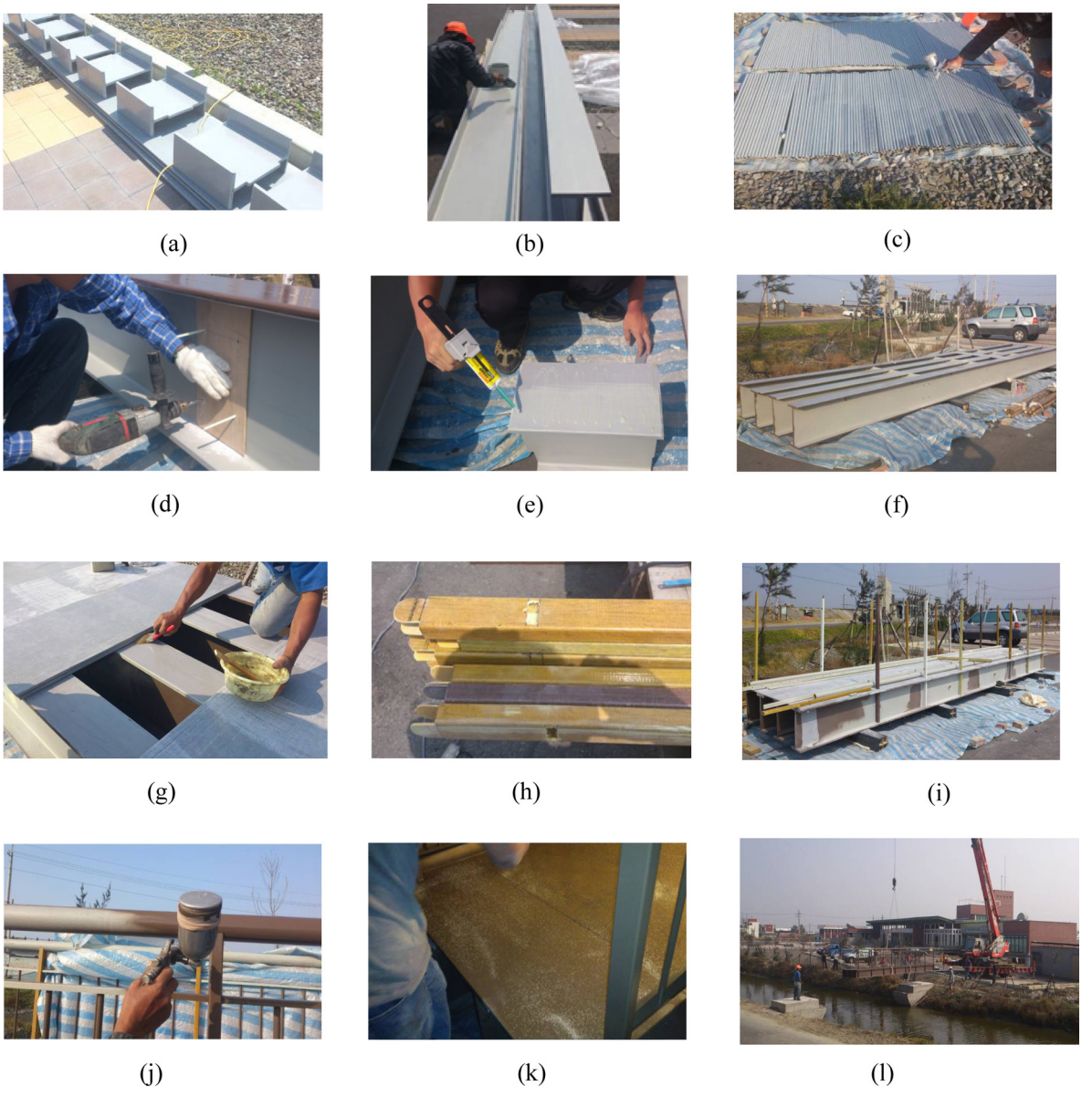


**Fig. 7.** Timeline of assembly and installation of the pedestrian bridge.

8. Exterior surfaces were finished by spraying on a dark brown paint (Fig. 7(j)) that harmonizes with the park's environment.
9. An anti-skid surface was made on the deck surface (Fig. 7(k)) by applying a layer of the high-strength epoxy resin adhesive to the floor and spreading sand onto it.
10. A small crane was used to install the completed superstructure unto the abutment, shown in Fig. 7(l).

## 5. Digital archiving

After the installation of the pedestrian bridge, an innovative technique was used to digitally document the bridge for future reference. As introduced earlier, a 3D terrestrial laser scanner was used for this process.

A terrestrial laser scanner is a surveying device that emits and receives laser pulses reflected back from objects. Using the time difference between the sending and receiving signals, precise locations and dimensions of the objects can be

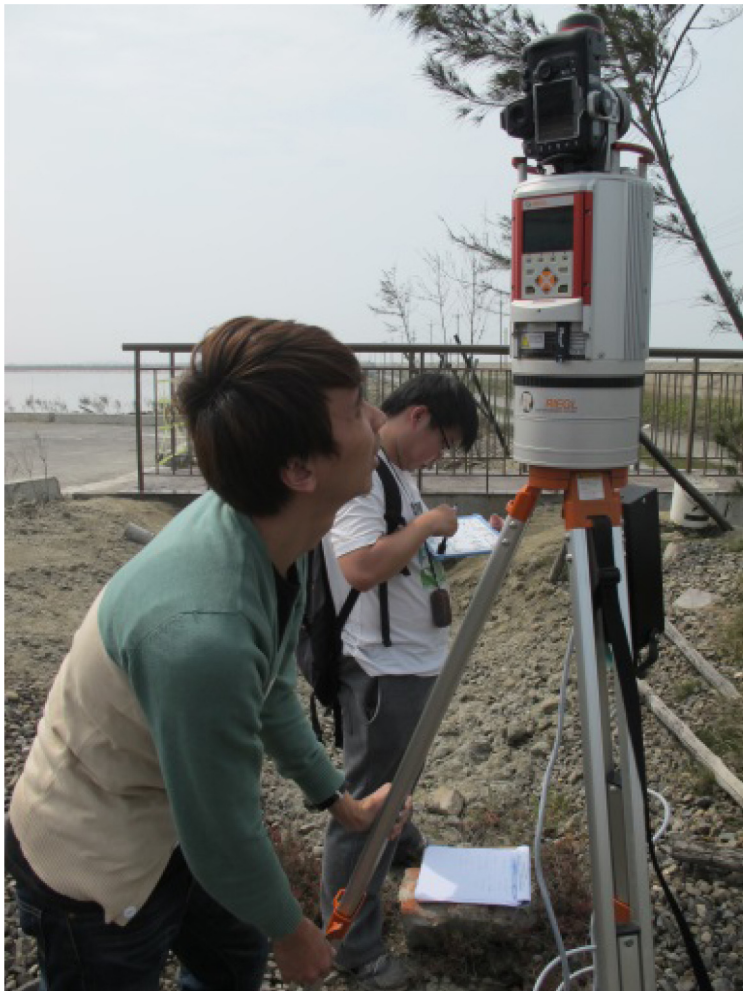

**Fig. 8.** Work photo of TLS scanning.

determined. In this study, a laser scanner manufactured by RIEGL (Fig. 8) was used to scan the pedestrian bridge (Wang et al., 2013). A total of seven scanning stations were set up around the bridge, and a vast amount of point clouds were recorded and used in the subsequent construction of a virtual model. These point clouds were collections of physical points (with *X*, *Y*, and *Z* coordinates) measured by the TLS. After the laser scanning, a computer program was used to merge the points into a virtual model of the pedestrian bridge (see Fig. 9). Once the virtual model was built for the bridge, many applications might take advantage of it. For example, the authors used the model to produce a tour video (completely generated by the computer) to showcase the bridge in different angles (Wang et al., 2013). The video also allowed the researchers to view and study the bridge from positions or locations normally not possible such as those high above the ground (to provide a bird's eye view without using aerial photography). The laser scanning is a great value-added tool that enhanced the understanding of the integration of the pedestrian bridge into the surrounding environment and the bridge structure itself. In addition to computer graphics and tour videos, other uses of the virtual model include scenario simulation, past and future comparison (for corrosion studies), virtual analysis of the bridge, and tourist promotion. The authors are believed to be the first to use the laser scanning technology in the National Parks of Taiwan.

## 6. Structural analysis

### *6.1. Theoretical analysis*

The superstructure of the bridge was analyzed and was made between the theoretical and numerical results of the pedestrian bridge. Eq. (1) for the Euler–Bernoulli Beam Theory (EBT) and Eqs. (2) and (3) (Ghugal and Sharma, 2011) of the Timoshenko Beam Theory (TBT) were employed to verify the accuracy of the FEA model of the pultruded GFRP girders. The

**Fig. 9.** Image computed by a computer using point clouds gathered by the TLS.

TBT was used to account for the effects of transverse shear. After the verification, the FEA model of the whole superstructure of the bridge was made.

$$\delta_{\max} = \frac{5wL^4}{384EI} \tag{1}$$

$$\delta_{\max} = \frac{5wL^4}{384EI} + \frac{wL^2}{8\kappa GA} \tag{2}$$

$$\delta_{\max} = \frac{5wL^4}{384EI}\left[1 + 1.92(1+\nu)\frac{h^2}{L^2}\right] \tag{3}$$

In the Eqs. (1)–(3), $\delta_{\max}$ is the maximum deflection; $w$ is the uniformly distributed load; $L$ is the span length of the girder; $I$ is the section moment of inertia, $G$ is the shear modulus; $A$ is the sectional area; and $\nu$ is the Poisson's ratio. The shear coefficient, $\kappa$, is obtained from Cowper (1996) for an I-section as:

$$\kappa = \left(\frac{10(1+\nu)(1+3m)^2}{(12+72m+150m^2+90m^3)+\nu(11+66m+135m^2+90m^3)+30n^2(m+m^2)+5\nu n^2(8m+9m^2)}\right) \tag{4}$$

where

$$m = \frac{2bt_{\text{flange}}}{ht_{\text{web}}} \tag{5}$$

$$n = \frac{b}{h} \tag{6}$$

Substituting Eqs. (5) and (6) into Eq. (4), we have $\kappa = 0.6$. The initial $b$ is the girder width; $h$ is the girder depth; $t_{\text{flange}}$ is the flange thickness; $t_{\text{web}}$ is the web thickness; and $\nu$ is the Poisson's ratio.

### 6.2. Finite element analysis

ANSYS was used for the FEA of the pedestrian bridge. The GFRP material is considered to have a linearly elastic behavior till failure. The Hooke's law constitutive relations for orthotropic GFRP material used in the FEA are in Eq. (7). Material properties provided in Table 1 for an orthotropic material were used in the FEA. The FEA models use an 8-noded SOLID 45

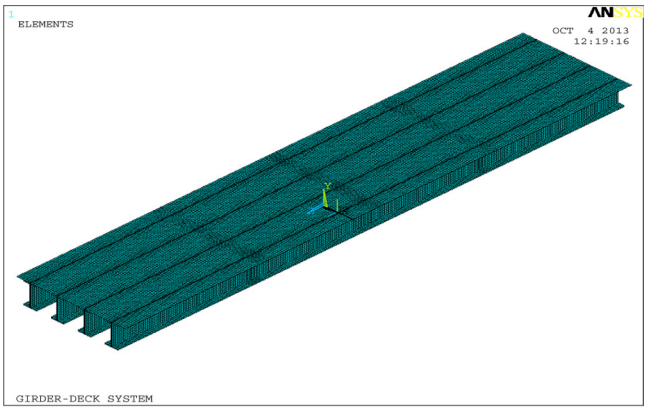


(a)

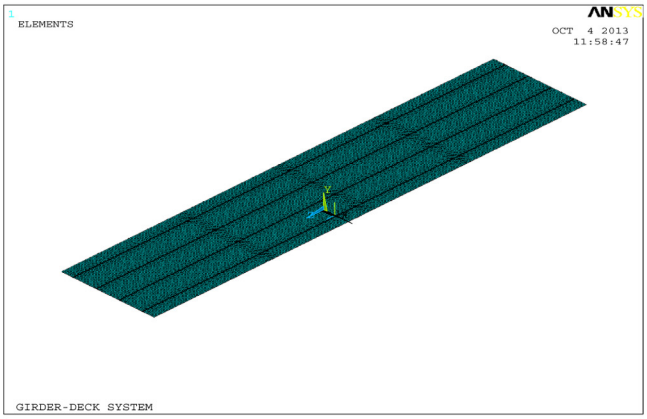


(b)

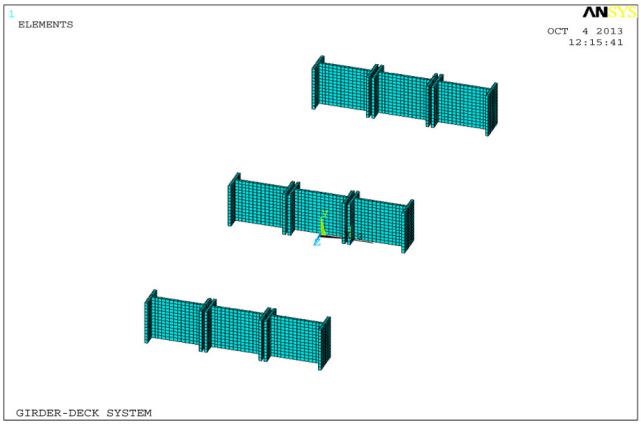


(c)

**Fig. 10.** FEA model of (a) girder-deck system, (b) deck and (c) diaphragm.

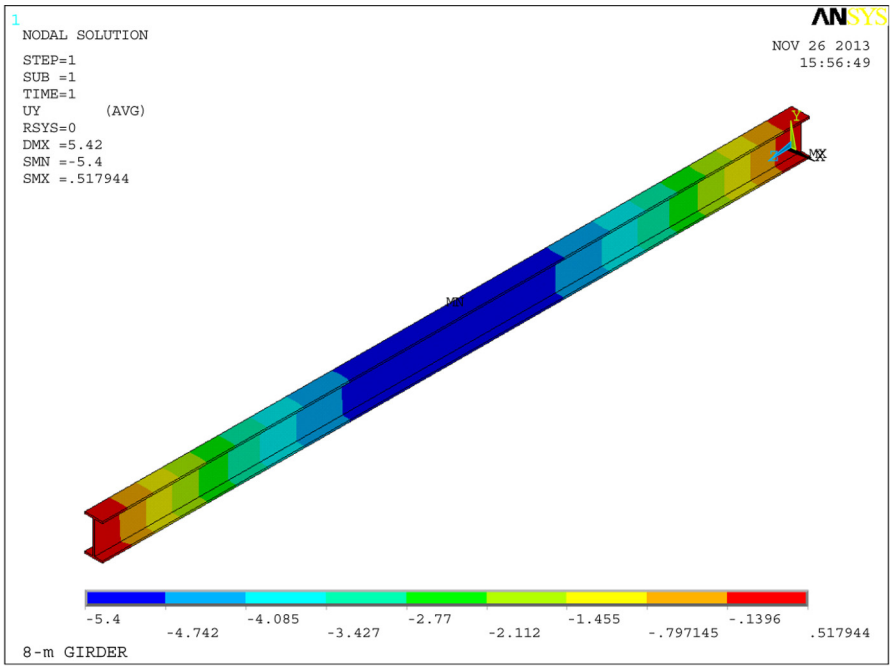


(a)

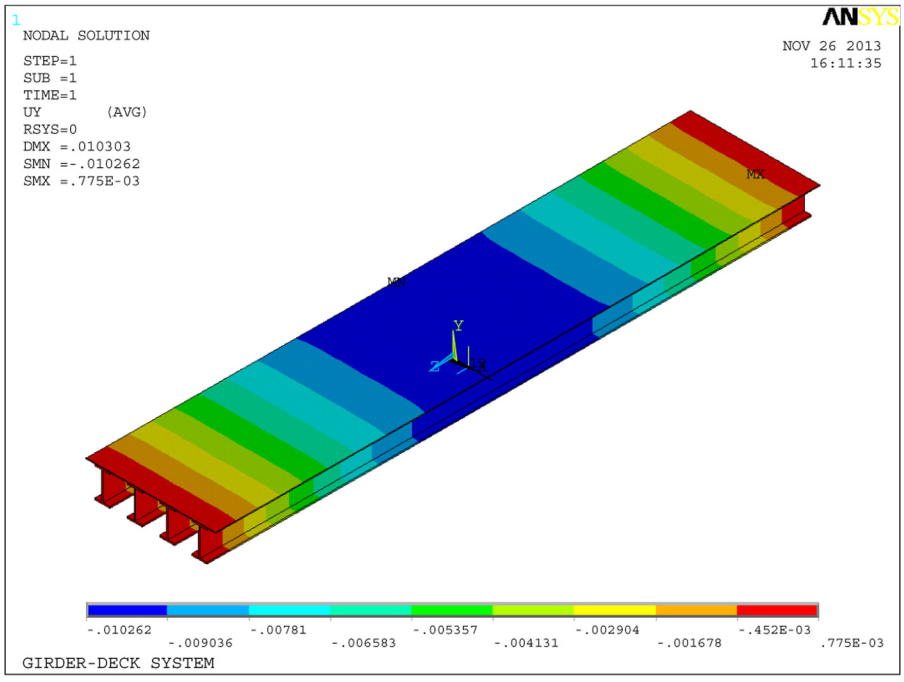


(b)

**Fig. 11.** Deflection contour of (a) 8-m girder and (b) girder-deck system.

**Table 3**
Deflection results from the analysis.

| Analytical methods | | 8-m girder (cm) | Girder-deck system (cm) | |
|---|---|---|---|---|
| FEA | | 0.542 | 1.03 | Meets deflection goal |
| EBT | | 0.539 | $L/500 = 1.5$ | |
| TBT | Ghugal and Sharma | 0.544 | | |
| | Eq. (2) | 0.562 | | |

element with 3 degrees of freedom at each node.

$$\begin{Bmatrix} \varepsilon_z \\ \varepsilon_x \\ \varepsilon_y \\ \gamma_{xz} \\ \gamma_{yz} \\ \gamma_{xz} \end{Bmatrix} = \begin{bmatrix} \frac{1}{E_z} & \frac{-\nu_{xz}}{E_x} & \frac{-\nu_{yz}}{E_y} & 0 & 0 & 0 \\ \frac{-\nu_{xz}}{E_z} & \frac{1}{E_x} & \frac{-\nu_{xy}}{E_y} & 0 & 0 & 0 \\ \frac{-\nu_{yz}}{E_z} & \frac{-\nu_{xy}}{E_x} & \frac{1}{E_y} & 0 & 0 & 0 \\ 0 & 0 & 0 & \frac{1}{G_{xy}} & 0 & 0 \\ 0 & 0 & 0 & 0 & \frac{1}{G_{yz}} & 0 \\ 0 & 0 & 0 & 0 & 0 & \frac{1}{G_{xz}} \end{bmatrix} \begin{Bmatrix} \sigma_z \\ \sigma_x \\ \sigma_y \\ \tau_{xy} \\ \tau_{yz} \\ \tau_{xz} \end{Bmatrix} \tag{7}$$

where

$$\frac{\nu_{yx}}{E_y} = \frac{\nu_{xy}}{E_x}, \frac{\nu_{zx}}{E_z} = \frac{\nu_{xz}}{E_x}, \frac{\nu_{zy}}{E_z} = \frac{\nu_{yz}}{E_y} \tag{8}$$

In Eqs. (7) and (8), subscripts $x$, $y$ and $z$ correspond, respectively, to the transverse, the vertical, and the longitudinal directions of the GFRP girder. The initial $\varepsilon$ stands for normal strain; $\gamma$ stands for shear strain; $\sigma$ is the normal stress; $\tau$ is the shear stress; $E$ is the Young's Modulus; $G$ is the shear modulus and $\nu$ is the Poisson's ratio.

Initially, an 8-m girder was analyzed first in ANSYS using a three-point bending condition and then the girder-deck system of the pedestrian bridge. The model of the girder-deck system in Fig. 10 included only the girders, deck and diaphragms. The parts were connected using a continuous mesh with shared common nodes and therefore a continuous stress is experienced between parts. Boundary conditions follow a simple support condition: a vertical displacement (in the $y$ direction) and transverse displacement ($x$ direction) restrain on the nodes of both ends; a z direction constraint at one of the ends. All loads were added as surface loads. A uniformly distributed load (4.07 kN/m$^2$) was applied on the deck of the girder-deck model as stipulated by *Guide Specifications for Design of FRP Pedestrian Bridges*, of the U.S. (AASHTO, 2008). Table 3 gives a comparison of the deflection value obtained from the analyses.

From Table 3, the deflection value for the FEA can be seen to be very close for the 8-m girder. Therefore, there was good agreement between the FEA results and the calculated theoretical results of the 8-m girders. This verifies the accuracy of the FEA model. Fig. 11 shows the deflection contours from ANSYS.

Since it is tedious using hand calculations for the deflection of the girder-deck system, the authors have used the deflection requirement of $L/500$ for the comparison. With a deflection value of only 1.03 cm from the FEA, the bridge has met the deflection goal of *Guide Specifications for Design of FRP Pedestrian Bridges*, U.S. (AASHTO, 2008).

## 7. Conclusions

Based on this study, the following conclusions can be drawn:

1. An all-GFRP composite pedestrian bridge consisted of superstructure, girders, decks, diaphragms, rods; and handrails made by GFRP composite materials was built in the high-chloride environment of the Taijiang National Park, Taiwan.
2. A Terrestrial Laser Scanner (TLS) was used to scan the pedestrian bridge and produce a 3D model of the bridge digitally for future reference.
3. From the analysis results of the 8-m girder, the deflection values for the EBT and TBT are very close when compared with the FEA result, thus verifying the accuracy of the FEA model.
4. The bridge was designed to meet the deflection goal of AASHTO's *Guide Specifications for Design of FRP Pedestrian Bridges* for a deflection not more than $L/500$. The pedestrian bridge met this deflection criterion and there was good correlation between the FEA results and the theoretical results.

## Acknowledgment

This work has been financially supported by the Construction and Planning Agency, Ministry of the Interior, Taiwan under contract number 101-A-103 with National Taipei University of Technology.

## References

American Association of State Highway and Transportation Officials (AASHTO). Guide specifications for design of FRP pedestrian bridges. 1st ed. Washington, DC: AASHTO; 2008.
American Association of State Highway and Transportation Officials (AASHTO). LRFD guide specifications for design of pedestrian bridges. 2nd ed. 2009.
Chen WW, Chang CH, Chung MK, Huang PS, Chung WT, Chung YL, Chen YW. Landslide site reconstruction with terrestrial laser scanning. In: The 18th International Conference on Geoinformatics (Geoinformatics 2010). Beijing, China, 18–20 June; 2010.
Chen HC, Chen WW, Chang CH. Novel in-situ method for fast determination of bridge pier displacements during push-over tests. Proc SPIE Int Soc Opt Eng 2011;8286. Art. No. 828623.
Cowper GR. The shear coefficient in Timoshenko's beam theory. J Appl Mech 1996;33(2):335–40.
Department of Agriculture, Forest Service, Technology & Development Program. A guide to fiber-reinforced polymer trail bridges. Missoula, MT: Department of Agriculture, Forest Service, Technology & Development Program; 2006.
Department for Transport. (sec. 3, Part 17, BD 90/05) Design of FRP Bridges and Highway Structures Design Manual for Roads and Bridges, vol. 1. London: Department for Transport; 2005.
Fiberline Composites Website accessed http://www.fiberline.com/structures/profiles-and-decks-bridges/profiles-footbridges-and-cycle-bridges/case-stories-footbridge/fiberline-bridge-kolding; October, 2013.
Ghugal YM, Sharma R. A refined shear deformation theory for flexure of thick beams. Latin Am J Solids Struct 2011;8(2):183–95.
Hsu CK, Chen WW. New landslide at Mt. Houshanyue Hiking Trail. In: International Symposium on Remote Sensing (ISRS 2013). Tokyo, Japan, 15–17 May; 2013.
Hsu CK, Chen WW. Topography analysis of Houshanyue Landslide. In: The 34th Asian Conference on Remote Sensing (ACRS 2013). Bali Indonesia, 20–24 October; 2013.
Japan Society of Civil Engineers. Guidelines for design and construction of FRP footbridges, Japan. 2011. (in Japanese).
Kayen R, Pack RT, Bay J, Sugimoto S, Tanaka H. Terrestrial-LIDAR visualization of surface and structural deformations of the 2004 Niigata Ken Chuetsu, Japan, earthquake. Earthq Spectra 2006;22(S1):147–62.
Kitayama N, Uno N. Design, fabrication and erection of the pedestrian bridge in the road-park of Ikei-Tairagawa in Okinawa. IHI Eng Rev 2003;36(2):35–9.
Kutz M. Construction applications of composites. In: Kutz M, editor. Handbook of materials selection. John Wiley& Sons; 2002, pp. 1415.
Liu WQ, Chen SE, Hauser E. LiDAR-based bridge structure defect detection. Exp Tech 2011;35(6):27–34.
Liu W, Chen SE, Hasuer E. Bridge clearance evaluation based on terrestrial LIDAR scan. J Perform Constr Facil ASCE 2012;26(4):469–77.
Pulroc Pultrusion Website accessed http://www.pulroc.com.tw/; December, 2013.
Skinner JM. A critical analysis of the Aberfeldy Footbridge, Scotland. In: Proceedings of bridge engineering 2 conference. University of Bath, Bath, UK, April; 2009.
Tang B, Podolny W Jr. A Successful beginning for fiber reinforced polymer (FRP) composite materials in bridge applications, FHWA. In: Proceedings, International Conference on Corrosion and Rehabilitation of Reinforced Concrete Structures. 7–11 Orlando, FL, December; 1998.
Tseng YT, Chou HT, Jhan YK, Wang JA, Chen WW. Laser scanning of the award-winning NTUT Green Gate. In: The 34th Asian Conference on Remote Sensing (ACRS). Bali, Indonesia, 20–24 October; 2013.
Wang JA, Hsu CK, Jhan YK, Chen WW, Li YF. Scanning of FRP passenger bridge in Taijiang National Park. Bali, IndonesiaIn: The 34th Asian Conference on Remote Sensing. 2013.
Watson C, Chen SE, Bian H, Hauser E. Three-dimensional terrestrial LIDAR for operational bridge clearance measurements. J Perform Constr Facil ASCE 2012;26(6):803–11.
Ye RQ, Niu RQ, Zhao YN, Jiang QY, Wu T. Integration of LIDAR data and geological maps for landslide hazard assessment in the three gorges reservoir area, China. In: Proceeding of the 18th International Conference on Geoinformatics: GIScience in Change, Geoinformatics. Peking University, Beijing, China, 18–20 June; 2010.